

Influence of the formation of intermetallics on the electrochemical properties of an $\text{Al}_{87}\text{Y}_5\text{Ni}_8$ amorphous alloy

L. BEDNARSKA^{1*}, T. MIKA², B. KOTUR², M. KOVBUZ¹, S. MUDRY³

¹ Department of Physical and Colloid Chemistry, Ivan Franko National University of Lviv, Kyryla i Mefodiya St. 6, 79005 Lviv, Ukraine

² Department of Inorganic Chemistry, Ivan Franko National University of Lviv, Kyryla i Mefodiya St. 6, 79005 Lviv, Ukraine

³ Department of Physics, Ivan Franko National University of Lviv, Kyryla i Mefodiya St. 8, 79005 Lviv, Ukraine

* Corresponding author. Tel.: +380-32-2728069; fax: +380-32-2978903; e-mail: L_Bednarska@franko.lviv.ua

Received October 15, 2007; accepted June 18, 2008; available on-line September 10, 2008

The influence of the formation of intermetallic compounds on the electrochemical properties of an $\text{Al}_{87}\text{Y}_5\text{Ni}_8$ amorphous metallic alloy (AMA) was investigated by means of differential scanning calorimetry (DSC), X-ray diffraction (XRD) and high-resolution electron microscopy (HREM). It is shown that the crystallization process taking place upon annealing can be subdivided into three stages corresponding to DSC maxima at 505, 602 and 632 K, respectively. The first and the second stage of crystallization were attributed to the formation of an fcc-Al(Y) solid solution in the amorphous matrix. During the third stage of crystallization precipitation of the fcc-Al(Y) solid solution and of the ternary compound $\text{Al}_{19}\text{Y}_3\text{Ni}_5$ with orthorhombic $\text{Al}_{19}\text{Gd}_3\text{Ni}_5$ -type structure was observed. An increase of the size of the precipitated phases reduces the corrosion rate coefficient b of the AMA.

Amorphous metallic alloy / Crystallization process / Corrosion resistance

1. Introduction

It is known that the duration and temperature of annealing of amorphous metallic alloys are responsible not only for structuring [1,2], but also for changes in the composition of the surface layers [3-5]. These two characteristics are related to physico-chemical features of the amorphous alloys and to their electrochemical corrosion resistance in particular. Amorphous Al-based alloys show higher chemical resistance in aggressive media than crystalline ones [6-8]. This is related to the absence of inhomogeneities on the surface of the alloys, since inhomogeneities promote the localization of surface energy and decrease the chemical resistance [6]. Heat treatment of amorphous alloys leads to the formation of nanocrystals, not only in the bulk but also on the sample surface, which in turn leads to an increase of the surface energy with respect to the amorphous state. This causes a decrease of the corrosion resistance of the annealed alloy in comparison with that of the initial amorphous sample.

The effect of pressure and temperature on the crystallization processes in $\text{Al}_{89}\text{La}_6\text{Ni}_5$ has been studied in [9,10]. The results obtained in [9] indicate

a two-step crystallization process for pressures up to 4 GPa. The first step, corresponding to the simultaneous precipitation of fcc-Al crystals and a metastable bcc-(Al,Ni)₁₁La₃-like phase, is governed by a eutectic reaction. The second step corresponds to the transformation of residual amorphous alloy into fcc-Al, $\text{Al}_{11}\text{La}_3$, Al_3Ni , and unidentified phases. Applied pressure strongly affects the crystallization process of the amorphous alloy. Both temperatures at which phase transformation occurs decreased with increasing pressure below 1 GPa and then increased for pressures up to 4 GPa. The results are discussed with reference to competing processes between the thermodynamic potential barrier and the diffusion activation energy under pressure. It was shown in [10] that time-dependent nucleation is observed in the amorphous alloy and the experimental data could be fitted by both Zeldovich's and Kashchiev's transient nucleation models with transient nucleation times of 220 and 120 min, respectively.

In this paper we present the results of an investigation of the correlation between corrosion resistance and the structure of an Al-based amorphous alloy $\text{Al}_{87}\text{Y}_5\text{Ni}_8$ as a function of the temperature of its heat treatment.

2. Experimental procedures

2.1. Materials

An amorphous $\text{Al}_{87}\text{Y}_5\text{Ni}_8$ alloy in form of a ribbon of about 30 μm thickness and 15 mm width was prepared by melt spinning in helium atmosphere with a cooling rate of $7 \cdot 10^5 \text{ K} \cdot \text{s}^{-1}$. The initial melt was prepared from a binary Al_3Y alloy and pure metals by induction melting. A crystalline ternary alloy $\text{Al}_{87}\text{Y}_5\text{Ni}_8$ and also the Al_3Y alloy were obtained by arc-melting technique in argon atmosphere. The purity of the initial metals was: Al – 99.999 wt.%, Y – 99.96 wt.%, Ni – 99.99 wt.%.

2.2. Methods

Differential scanning calorimetry (DSC). The structure changes of the AMA during the heat treatment were studied by means of DSC (Perkin-Elmer Pyris 1) with a heating rate of $20 \text{ K} \cdot \text{min}^{-1}$.

X-ray diffraction (XRD). Phase identification and determination of the crystallographic parameters of the intermetallic phases that appear during crystallization of the AMA were carried out by X-ray diffraction (X'Pert Philips PW 3040 diffractometer, Cu-K_α radiation obtained using a graphite monochromator on the reflected beam, 2θ range: 10° – 140° , scan step 0.04°). A Rietveld profile analysis was applied (standard FullProf program) for the calculation of the parameters of the nanocrystals. For the study of the primary crystallization, the samples were annealed for 1 h at 532, 612 and 639 K before the XRD-studies. These temperatures were determined as 5 K above the temperature of the end of the first DSC maximum.

Electrochemical testing. The corrosive behaviour of amorphous and crystalline $\text{Al}_{87}\text{Y}_5\text{Ni}_8$ alloys in an 1.5 % NaCl aqueous solution was investigated. Measurements of the $i = f(E)$ (where i is the current density in $\mu\text{A} \cdot \text{cm}^{-2}$, E the polarization potential in mV) dependence were carried out using an IMP88PC-R potentiostat. Polarization curves were obtained under a potentiodynamical regime with a scanning time 1 s per point. The scanning rate of the potential $\Delta E/\Delta t$ was $20 \text{ mV} \cdot \text{s}^{-1}$. A saturated calomel electrode (SCE) was used as reference electrode for all the electrochemical studies.

High-resolution electron microscopy (HREM). HREM (JEM 3010 microscope) was used for visual observation of the samples before and after the heat treatment of the AMA.

Microprobe analysis. Microprobe analysis of the AMA was conducted on a REMMA-102-02 electron microprobe analyzer (scanning step– $20 \mu\text{m}$).

3. Results and Discussion

3.1. Structural changes of the $\text{Al}_{87}\text{Y}_5\text{Ni}_8$ amorphous alloy

The DSC curve obtained for the examined $\text{Al}_{87}\text{Y}_5\text{Ni}_8$ amorphous alloy (heating rate $20 \text{ K} \cdot \text{min}^{-1}$) is shown in

Fig. 1. Crystallisation occurs in three stages (I–III). It can be seen that primary crystallization takes place in the temperature range 495–527 K (maximum at 505 K) with an enthalpy of formation of nanocrystals $\Delta H_{\text{I}} = -22.8 \text{ J} \cdot \text{g}^{-1}$. Two other, more intense and sharper peaks (II and III) on the DSC curve are observed in the temperature ranges 601–607 and 629–634 K, with maxima at 602 and 632 K, respectively. Such peaks are typical for eutectic crystallization and are in our case characterized by the enthalpy values $\Delta H_{\text{II}} = -42.1 \text{ J} \cdot \text{g}^{-1}$ and $\Delta H_{\text{III}} = -72.5 \text{ J} \cdot \text{g}^{-1}$, respectively. Three similar exothermic peaks were observed for $\text{Al}_{87}\text{Y}_7\text{Fe}_5$ by Boucharat *et al.* [11].

In order to study the primary crystallization, all samples were annealed for 1 h at temperatures determined as 5 K above the temperature of the end of the first DSC maximum (see Fig. 1). Fig. 2 represents the X-ray diffraction patterns obtained for the examined alloys in the as-quenched state and after heat treatment

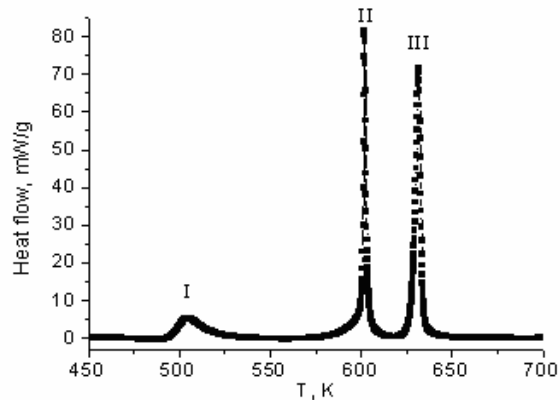


Fig. 1 DSC curve for the $\text{Al}_{87}\text{Y}_5\text{Ni}_8$ amorphous alloy (heating rate: $20 \text{ K} \cdot \text{min}^{-1}$).

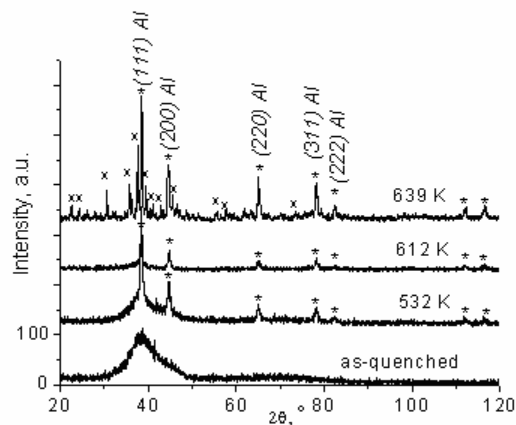


Fig. 2 XRD patterns of the examined alloys annealed for 1 h at different temperatures. Markers show the reflections corresponding to fcc-Al (*) and $\text{Al}_{19}\text{Y}_3\text{Ni}_5$ (x).

at 532, 612 and 639 K. The sharp Al diffraction peaks and the diffuse scattering indicate that annealing causes the formation of a solid solution of Y in fcc-Al nanograins, embedded in an amorphous Al(Y) matrix. The diffraction pattern obtained at $T=532$ K (Fig. 2) exhibits (111), (200), (220), (311), and (222) diffraction peaks of the fcc-lattice of aluminium on the background of the diffusion maximum of the amorphous phase. An increase of the annealing temperature leads to an increase of the integrated intensities and a decrease of the width of the peaks, which indicates an increase of the size of the Al nanocrystals and of their volume fraction in the sample [12].

The diameter of the Al nanocrystals in the amorphous matrix after the first stage of alloy crystallization, determined from the HREM image (Fig. 3), is about 15–17 nm. The inhomogeneous distribution of the dots on the HREM image indicates that redistribution of the metal atom occurs in the amorphous matrix during low-temperature annealing. Areas that are enriched by Y-atoms arise and increase with time under these conditions. Since the atomic diameter of Y, D_Y (0.360 nm), is larger than that of Al, D_{Al} (0.286 nm), the presence of Y-atoms delays the diffusion of Al-atoms and, as a result, limits the size of the nanograins of the initial phase.

The second stage of crystallization was attributed to the formation, from the amorphous matrix, of a new fraction of nanograins with 20 nm diameter. This formation of a eutectic mixture of Al nanocrystals and the Al_3Ni intermetallic compound from the amorphous matrix takes place in the temperature interval 601–607 K. These results were obtained from XRD-data (see Fig. 2) and have been published in more detail elsewhere [13]. During the third stage of crystallization, precipitation of the fcc-Al(Y) solid solution and a ternary compound, $Al_{19}Y_3Ni_5$ with orthorhombic $Al_{19}Gd_3Ni_5$ -type structure, was observed.

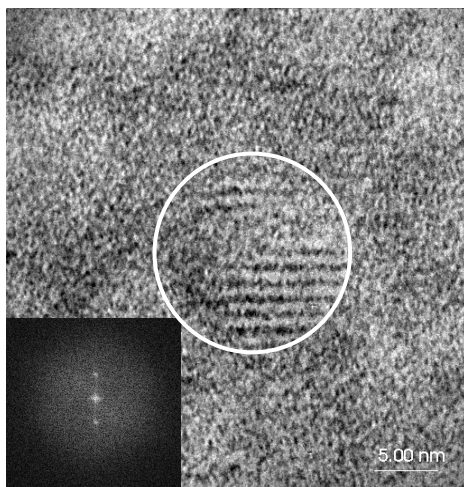


Fig. 3 HREM image of the $Al_{87}Y_5Ni_8$ sample heated up to 532 K with a heating rate of $20\text{ K}\cdot\text{min}^{-1}$. A circle indicates the nanocrystalline area.

3.2. Corrosion behaviour of $Al_{87}Y_5Ni_8$ after annealing

The electrochemical properties of AMA depend not only on the composition but also on the structural state. Low-temperature annealing at 373 K leads to diffusion of metal atoms in the amorphous matrix and favors a redistribution of the elements in the layers near the surface, which is reflected on the electrochemical characteristics of the $Al_{87}Y_5Ni_8$ dissolution-ionization. The intermetallic compounds that form during annealing at temperatures corresponding to the different crystallization stages, have a significant influence on the electrochemical activity of $Al_{87}Y_5Ni_8$. Therefore, a comparative electrochemical testing of electrodes made from Al (99.999% purity), arc-melted $Al_{87}Y_5Ni_8$ alloy, initial $Al_{87}Y_5Ni_8$ AMA, and of the latter sample annealed at 373, 532, 612, and 639 K, was carried out. The potentiodynamic polarization curves obtained for these samples are shown in Fig. 4. The curves 1 and 2 show that doping of crystalline Al with Y and Ni significantly changes the electrochemical parameters and the oxidation has shifted the values of the corrosion potential from -847 mV to -567 mV.

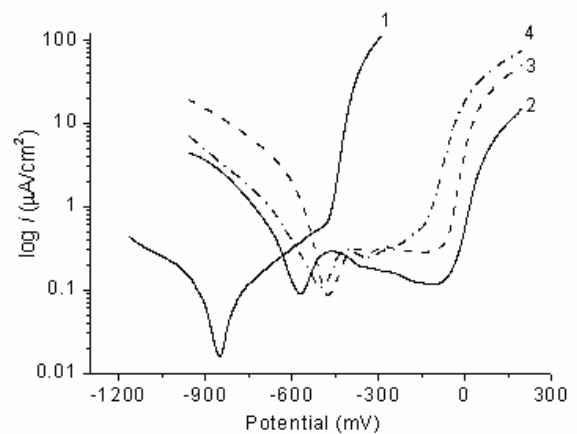


Fig. 4 Potentiodynamic polarization curves (polarization time ~ 150 s) in 1.5 % NaCl aqueous solution for crystalline Al (1), an arc-melted $Al_{87}Y_5Ni_8$ alloy (2), an amorphous $Al_{87}Y_5Ni_8$ alloy (3), and the amorphous $Al_{87}Y_5Ni_8$ alloy annealed at 612 K (4).

The electrochemical processes taking place on the surface of the arc-melted polycrystalline sample, the initial amorphous sample and the $Al_{87}Y_5Ni_8$ AMA annealed at 612 K (curves 2–4 in Fig. 4) differ significantly from those taking place in pure Al (curve 1). The wide interval of passivation (from -450 to -150 mV) points on the effective protection of oxide films on the surface for all the $Al_{87}Y_5Ni_8$ samples. The corrosion potential of the amorphous $Al_{87}Y_5Ni_8$ alloy is equal -485 mV, which indicates that amorphization also leads to an improvement of the corrosive resistance properties.

Annealing of the amorphous alloy at 373 K for 1 h enhances significantly the corrosive resistance as a consequence of the changes of the composition

Table 1 Electrochemical parameters of corrosion of the $\text{Al}_{87}\text{Y}_5\text{Ni}_8$ samples in 1.5 % NaCl aqueous solution.

Sample $\text{Al}_{87}\text{Y}_5\text{Ni}_8$	$E_{\text{corr.}}$, mV	$i_{\text{corr.}}$, $\mu\text{A}\cdot\text{cm}^{-2}$	$\Delta E_{\text{pass.}}$, mV	$i_{\text{pass.}}$, $\mu\text{A}\cdot\text{cm}^{-2}$	$E_{\text{pit.}}$, mV
in as-quenched state	-485	0.06	395	0.30	-49
annealed at T_a , K	373	0.006	522	0.03	-54
	532	0.029	309	0.02	-92
	612	0.035	238	0.04	-129
	639	0.93	236	0.25	-134
arc-melted alloy	-485	0.07	353	0.17	-54

of the sample surface. According to the results of the microprobe analysis the layers near the surface of the initial sample and after annealing at 373 and 532 K contained 73.25, 68.81 and 70.87 wt.% Al, respectively (21.42 wt.% Ni). During annealing also the oxidative processes on the surface of the AMA are activated and a stable protective layer is formed. This is confirmed by a sharp decrease of the corrosive current $i_{\text{corr.}}$ (from 0.06 to 0.006 $\mu\text{A}\cdot\text{cm}^{-2}$) and an increase by 125 mV of the passivation interval $\Delta E_{\text{pass.}}$ for the sample annealed at 373 K in comparison with the initial sample (see Table 1). It must also be noted that the values of the corrosion potential $E_{\text{corr.}}$ and pitting potential $E_{\text{pit.}}$ for the AMA annealed at 373 K and the arc-melted $\text{Al}_{87}\text{Y}_5\text{Ni}_8$ alloys are identical. This suggests the possible formation of a passivation oxide layer on the surface of both samples.

The as-quenched amorphous sample and the sample annealed at 639 K are characterised by the same corrosion potential, $E_{\text{corr.}} = -485$ mV. However, the values of the corrosion current $i_{\text{corr.}}$ of these samples differ significantly: 0.06 $\mu\text{A}\cdot\text{cm}^{-2}$ and 0.93 $\mu\text{A}\cdot\text{cm}^{-2}$, respectively. Such a sharp increase of the corrosion current density and passivation are related to the considerable increase of the content of crystalline Al_3Ni and $\text{Al}_{19}\text{Y}_3\text{Ni}_5$ phases in the annealed sample.

An analysis of the data obtained here and literature data for other Al-based alloys [14,15] allowed us to conclude that protective oxide films change the corrosion resistance in the 1.5 % NaCl aqueous solution. Dense oxide films are formed on the surface of the AMA at 612 K by electrochemical interaction of the sample with the 1.5 % NaCl aqueous solution. In this case a small corrosion current ($\sim 0.035 \mu\text{A}\cdot\text{cm}^{-2}$) was observed.

The thermal treatment of the AMA under investigation influences both the crystallization of the intermetallic phases and the size of the nanocrystals [13]. This is shown in Fig. 5, where the dependence of the electrochemical parameter b on the annealing temperature is presented. The parameter b is proportional to the corrosion rate and was calculated from voltammometric measurements according to the formula: $b = (\log i_2 - \log i_1) / (E_2 - E_1)$. Formation of nanocrystals with a size >50 nm occurs as a mixture of solid solution Al(Y) and the ternary compound

$\text{Al}_{19}\text{Y}_3\text{Ni}_5$ during annealing of the AMA at $T = 639$ K. In this case the contact of the AMA with the aggressive medium (1.5 % NaCl aqueous solution) leads to the formation of more defective oxide films on the surface and to an extreme increase of the electrochemical activity (Table 1).

Consequently, the changes of the electrochemical parameters during the thermal treatment are caused mainly by the degree of structuring in the amorphous alloy. As it is shown in Fig. 5, the corrosive rate remains unchanged in the temperature interval 293–373 K, while the electrochemical characteristics (see Table 1) indicate protective properties due to surface oxide layers.

The electrochemical parameter b changes significantly at $T \geq 532$ K, after the first stage of AMA crystallization. After the stages II and III of crystallization the surface of the AMA is close to thermodynamic equilibrium and, as a result, the electrochemical parameter b shows lower values. Formation of the ternary compounds Al_3Ni and $\text{Al}_{19}\text{Y}_3\text{Ni}_5$ during the stages II and III of crystallization, respectively, which takes place simultaneously with formation of an fcc solid solution Al(Y), leads to an increase of the corrosion current and of the electrochemical parameter b .

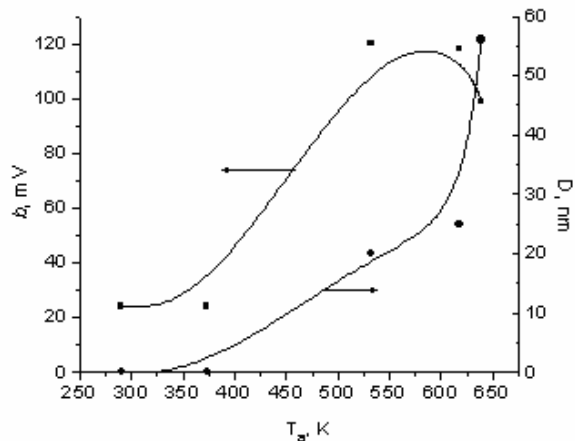


Fig. 5 The crystallite diameter (D) and the electrochemical parameter (b) for different annealing temperatures (T_a) of amorphous $\text{Al}_{87}\text{Y}_5\text{Ni}_8$ alloys.

4. Conclusions

Crystallization of $\text{Al}_{87}\text{Y}_5\text{Ni}_8$ amorphous alloys proceeds in three stages corresponding to $T = 505$ K, 602 K and 632 K. Formation of an fcc-Al(Y) solid solution is observed during stages I and II. The third stage corresponds to the formation of fcc-Al(Y) and a ternary compound, $\text{Al}_{19}\text{Y}_3\text{Ni}_5$ ($\text{Al}_{19}\text{Gd}_3\text{Ni}_{15}$ -type structure). Annealing at different temperatures up to 612 K promotes the formation of small Al(Y) crystallites, randomly distributed in the amorphous matrix. Dense protective films were formed on the AMA surface before and after annealing process at 612 K during their interaction with an 1.5 % NaCl aqueous solution. The contact of the same aggressive medium with an alloy annealed at a higher temperature (639 K) led to the formation of more defective oxide films. The significant changes of the electrochemical parameters observed after the thermal treatment are caused mainly by changes of the degree of structuring in the initially amorphous alloy.

Acknowledgements

The authors are thankful to Dr V. Nosenko for help in the preparation of amorphous ribbons. The present work was supported in part by the Ministry of Education and Science of Ukraine, Grant No. 0106U001325. We are also grateful to our collaborators from the Institute of Physics and Chemistry of Materials of the Silesian University (Poland) for the DSC measurements.

References

- [1] A. Inoue, *Acta Mater.* 48 (2000) 279.
- [2] A.N. Mansour, C.A. Melendres, *J. Electrochem. Soc.* 142 (1995) 1961.
- [3] E. Van Gheem, J. Vereecken, C. Le Pen, *J. Appl. Electrochem.* 32 (2002) 1193.
- [4] A.V. Benedetti, P.L. Cabot, J.A. Garrido, A.H. Moreira, *J. Appl. Electrochem.* 31 (2001) 293.
- [5] A. Inoue, *Prog. Mater. Sci.* 43 (1998) 365.
- [6] D. Bowlin, A. Scheeline, A. Pearlstein, *Electrochem. Acta* 43 (1998) 417.
- [7] M. Seruga, D. Hasenay, *J. Appl. Electrochem.* 31 (2001) 961.
- [8] C. Monticelli, F. Zucchi, G. Brunoro, G. Trabanelli, *J. Appl. Electrochem.* 27 (1997) 325.
- [9] Y.X. Zhuang, J.Z. Jiang, T.J. Zhou, H. Rasmussen, L. Gerward, M. Mezouar, W. Crichton, A. Inoue, *Appl. Phys. Lett.* 77(25) (2000) 4133.
- [10] Y.X. Zhuang, J.Z. Jiang, Z.G. Lin, M. Mezouar, W. Crichton, A. Inoue, *Appl. Phys. Lett.* 79(6) (2001) 743.
- [11] N. Boucharat, H. Rosner, R. Valiev, G. Wilde, *Arch. Mater. Sci.* 25 (2004) 357.
- [12] A.G. Ilinsky, A.G. Maslov, V.K. Nosenko, A.P. Brovko, I.K. Yevlash, *Met. Phys. Adv. Technol.* 21(12) (1999) 38.
- [13] T. Mika, M. Karolus, G. Haneczok, L. Bednarska, E. Łagiewka, B. Kotur, *J. Non-Cryst. Solids* 354 (2008) 3099.
- [14] N.N. Aung, W. Zhou, *J. Appl. Electrochem.* 32 (2002) 1397.
- [15] A.A. Mazhar, S.T. Arab, E.A. Noor, *J. Appl. Electrochem.* 31 (2001) 1131.